UNIVERSITY OF LEEDS

This is a repository copy of *Undrained cavity expansion analysis with a unified state parameter model for clay and sand*.

White Rose Research Online URL for this paper:
http://eprints.whiterose.ac.uk/112518/

Version: Accepted Version

Article:
Mo, PQ and Yu, HS orcid.org/0000-0003-3330-1531 (2017) Undrained cavity expansion analysis with a unified state parameter model for clay and sand. Géotechnique, 67 (6). pp. 503-515. ISSN 0016-8505

https://doi.org/10.1680/jgeot.15.P.261

Reuse
Items deposited in White Rose Research Online are protected by copyright, with all rights reserved unless indicated otherwise. They may be downloaded and/or printed for private study, or other acts as permitted by national copyright laws. The publisher or other rights holders may allow further reproduction and re-use of the full text version. This is indicated by the licence information on the White Rose Research Online record for the item.

Takedown
If you consider content in White Rose Research Online to be in breach of UK law, please notify us by emailing eprints@whiterose.ac.uk including the URL of the record and the reason for the withdrawal request.

White Rose university consortium
Universities of Leeds, Sheffield & York

eprints@whiterose.ac.uk
https://eprints.whiterose.ac.uk/

Undrained cavity expansion analysis with a unified state parameter model for clay and sand

P. Q. MO* and H. S. YU†

This paper presents a new analytical solution for undrained expansion of spherical and cylindrical cavities in soils with a unified state parameter model for clay and sand (CASM). Large strain and effective stress solutions are derived for soils in the elastic, plastic and critical-state regions. The key advantage of using the state parameter model CASM is that it can model both clay and sand and is generally able to capture overall soil behaviour as observed in the laboratory. The newly developed solution provides the stress and strain fields during the expansion of a cavity from an initial to a final radius. Following the validation with the original Cam Clay solution, a simple parametric study is conducted to investigate the effects of key model parameters on stress distributions and cavity expansion curves. Applications to the analysis of pile installation and self-boring pressuremeter tests highlight some important implications in geotechnical practice.

KEYWORDS: in situ testing; plasticity; stress path; theoretical analysis

INTRODUCTION

Cavity expansion theory has been extensively developed and widely applied to geotechnical problems, such as in situ soil testing, pile foundation and tunnelling (Yu, 2000). In addition to classical cavity expansion solutions in elastic materials, a range of analytical solutions have been proposed using more sophisticated constitutive soil models, from elastic perfectly plastic soils (Vesic, 1972; Carter *et al.*, 1986; Yu & Houlsby, 1991; Mo *et al.*, 2014) to elastic plastic strain hardening soils (Palmer & Mitchell, 1971; Collins & Yu, 1996; Chen & Abousleiman, 2012, 2013). Although numerical simulations are gaining popularity for boundary value problems when sophisticated soil models are employed (Carter, 1978; Yu, 1990; Yu *et al.*, 2005), analytical solutions remain highly useful both for validation of numerical simulations and providing insight into the relative importance of various soil parameters.

As the most widely used strain-hardening/softening models in soil mechanics and geotechnical engineering, critical state soil models (Schofield & Wroth, 1968) have been used to derive cavity expansion solutions under both drained and undrained conditions in the past two decades. Similarity solutions for drained and undrained cavities from zero initial radius in critical state soils were presented by Collins *et al.* (1992) and Collins & Stimpson (1994), and these provided predictions of the limit effective cavity pressure and excess pore pressure for both spherical and cylindrical cavities. Subsequently, Collins & Yu (1996) presented a complete large strain solution procedure for cavity expansion from an arbitrary initial radius in a variety of Cam-clay critical state soils. The general effective stress analyses for large strain cavity expansions were provided with simple quadratures. Analytical effective stress solutions were derived, but only for the original Cam clay. These critical state solutions were applied to a pile installation (Collins & Yu, 1996) and a self-boring pressuremeter (Yu & Collins, 1998). Cao *et al.* (2001) presented an analysis of the undrained expansion of a cavity in modified Cam clay, by applying small strain in the elastic zone and large strain in the plastic zone. More recently, further semi-analytical solutions for undrained and drained expansions of cylindrical cavities in modified Cam clay soils have been reported by Chen & Abousleiman (2012) and Chen & Abousleiman (2013). By introducing an out-of-plane in situ stress around the cylindrical cavity, the solutions removed the limitation on the initial condition of isotropic stress state, in order to simulate the more general case where the in situ vertical stress may be different from the horizontal one. However, in terms of constitutive models, there have been difficulties in modelling heavily overconsolidated clays using critical state models, and most critical state models were used with an associated flow rule, which showed very low accuracy for prediction of soil behaviour in loose sand and normally consolidated clays. In consideration of the limitations for modelling granular materials using conventional critical state models, cavity expansion solutions with a unified soil model for clay and sand are still not available.

In this paper a novel analytical effective stress solution for undrained expansion in both spherical and cylindrical cavities in a unified state parameter model for clay and sand (CASM), developed by Yu (1998), is presented. After introducing the unified state parameter model with Rowe's stress dilatancy relation, the complete large strain analyses are provided for soil in elastic, plastic and critical-state regions. The solution is then validated against the existing results for the original Cam-clay model. Further results on stress paths, stress distributions and cavity expansion curves are investigated with the variation of soil parameters and overconsolidation ratio. Brief applications to pile installation and self-boring pressuremeter are also provided, followed by concluding remarks.

PROBLEM DEFINITION

The present paper is concerned with the expansion of a spherical/cylindrical cavity with initial radius a_0 in an infinite soil under undrained conditions. The geometry and kinematics of cavity expansion are illustrated schematically in

Manuscript received 23 November 2015; revised manuscript accepted 14 November 2016.
Discussion on this paper is welcomed by the editor.
* State Key Laboratory for GeoMechanics and Deep Underground Engineering, China University of Mining and Technology, Xuzhou, Jiangsu, P. R. China.
† School of Civil Engineering, University of Leeds, Leeds, UK.

Fig. 1. The initial stress state is isotropic (i.e. $\sigma'_{r,0} = \sigma'_{\theta,0} = p'_0$; for the cylindrical case, $\sigma'_{z,0}$ is also equal to p'_0), with initial ambient pore pressure u_0. The preconsolidation pressure is referred to as p'_{y0}, and $R_0 = p'_{y0}/p'_0$ represents the isotropic overconsolidation ratio in terms of the mean effective stress. The initial specific volume is referred to as v_0, and the specific volume remains constant ($v = v_0$) during the process of expansion for undrained analysis. Note that a compression positive notation is used in this paper.

For cavity expansion problems, the quasi-static equilibrium equation can be written as

$$\sigma_\theta - \sigma_r = \frac{r}{m}\frac{\partial \sigma_r}{\partial r} \tag{1}$$

where the parameter 'm' is used to integrate both spherical ($m = 2$) and cylindrical ($m = 1$) scenarios; σ_r and σ_θ are the total radial and tangential stresses, and r is the radius of the material element (r_0 is the initial position before cavity expansion). Excess pore pressure Δu is calculated as $u - u_0$. In terms of spherical and cylindrical scenarios, the mean and deviatoric effective stresses (p'; q) for cavity expansion problems can be defined as follows

$$\begin{aligned} p' &= \frac{\sigma'_r + m\sigma'_\theta}{1+m} \\ q &= \sigma'_r - \sigma'_\theta \end{aligned} \tag{2}$$

Similarly, the volumetric and shear strains (δ; γ) are expressed as

$$\begin{aligned} \delta &= \varepsilon_r + m\varepsilon_\theta = 0 \\ \gamma &= \varepsilon_r - \varepsilon_\theta \end{aligned} \tag{3}$$

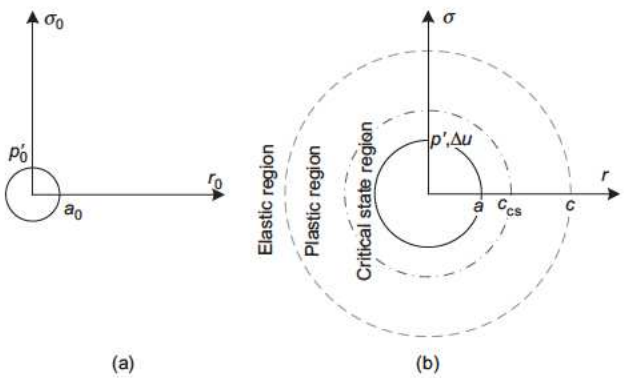

Fig. 1. Geometry and kinematics of cavity: (a) initial cavity before expansion; (b) cavity after expansion

The definitions of 'q' provided in equation (2) and 'γ' in equation (3) are used in this paper mainly to simplify the solution procedures to enable analytical solutions to be achieved. They are consistent with the solution of Collins & Yu (1996). It is recognised that, for the case of cylindrical cavities with an anisotropic in situ stress state, they are a simplified version of the three-dimensional (3D) critical state variables. However, for the isotropic in situ stress state (which is the problem addressed by this paper), the possible error introduced by this simplification has been shown to be negligible by a rigorous numerical (finite-element) simulation (Sheng *et al.*, 2000). This point was also considered and supported theoretically by Chen & Abousleiman (2012).

It is assumed that, while yielding occurs, the strains are decomposed additively into elastic and plastic components. Superscripts 'e' and 'p' are used to distinguish the elastic and plastic components of the total strains. To accommodate the effect of large deformation in the cavity expansion process, large strain analysis is adopted for both elastic and plastic regions by assuming logarithmic strains

$$\begin{aligned} \varepsilon_r &= -\ln\left(\frac{\mathrm{d}\,r}{\mathrm{d}\,r_0}\right) \\ \varepsilon_\theta &= -\ln\left(\frac{r}{r_0}\right) \end{aligned} \tag{4}$$

UNIFIED STATE PARAMETER MODEL

This section gives a brief description of the unified state parameter model CASM as developed by Yu (1998).

The concept of critical states has been adopted for the development of soil constitutive models since the 1950s (e.g. Parry, 1956; Roscoe *et al.*, 1958; Wroth, 1973). At critical state, soil behaves as a frictional fluid with constant volume and stresses; and the critical state line (CSL) is unique for a given soil regardless of the stress path (Schofield & Wroth, 1968), which is fully defined as

$$\begin{aligned} q &= M\,p' \\ v &= \Gamma - \lambda\,\ln p' \end{aligned} \tag{5}$$

where q and p' are the deviatoric and mean effective stresses; M is the slope of the critical state line in p' q space; $v = 1 + e$ is the specific volume, and e is the void ratio; λ, κ and Γ are critical state constants (see Fig. 2).

The Cam-clay model, developed by Roscoe & Schofield (1963), is one of the earliest and the most commonly used elastic plastic critical state models, which also has served as a

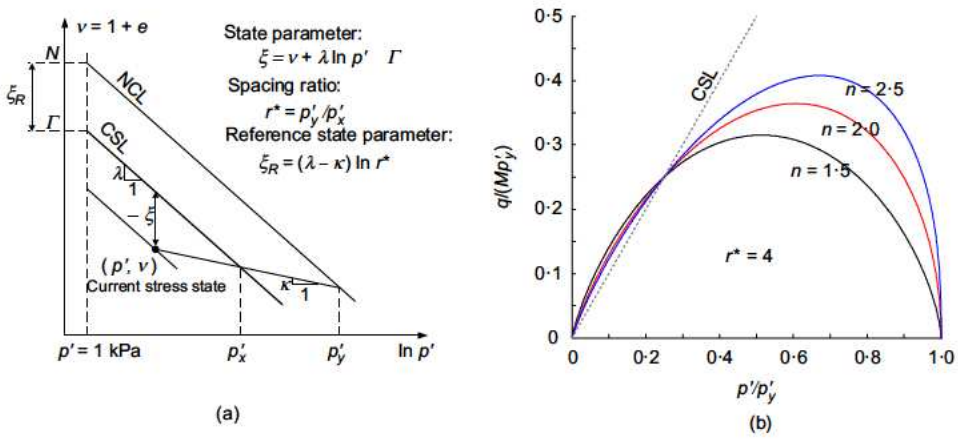

Fig. 2. A general stress state relation for both clay and sand in: (a) $\ln p' - v$ space (schematic diagram of state parameter); (b) p'/p'_y $q/(M\,p'_y)$ space (state boundary surfaces normalised by preconsolidation pressure)

standard model for modifications to describe soil behaviour. However, the critical state models were mostly limited to saturated clays and silts; the yield surfaces overestimated the failure stresses on the 'dry side'; and granular materials were rarely modelled by critical state models (Yu, 1998, 2006).

The state parameter ξ is defined by Been & Jefferies (1985) as the difference of specific volume between the current and critical states at the same mean effective stress (see Fig. 2(a))

$$\xi = v + \lambda \ \ln p' - \Gamma \tag{6}$$

It has shown its ability to describe the behaviour of granular material over a wide range of stresses and densities (Been & Jefferies, 1985; Sladen *et al.*, 1985; Sladen & Oswell, 1989). It is also established that the state parameter can be used to determine the soil responses for both clay and sand (Yu, 1998).

With the benefits of the concept of state parameter, Yu (1998) proposed a unified state parameter model for clay and sand, which is referred to as CASM. It is a simple constitutive model with two additional material constants introduced to the standard Cam-clay model, whereas the overall behaviour of clay and sand can be satisfactorily modelled by CASM under both drained and undrained loading conditions.

The state boundary surface of CASM is described as

$$\left(\frac{\eta}{M}\right)^n = 1 - \frac{\xi}{\xi_R} \tag{7}$$

where $\eta = q/p'$ is known as stress ratio; n is the stress-state coefficient, which is a new material constant and typically between approximately 1·0 and 5·0; $\xi_R = (\lambda - \kappa)\ln r^*$ is the reference state parameter; and r^* is the spacing ratio, defined as p'_y/p'_x (Fig. 2(a)). Equation (7) also represents the stress-state relation and the yield function. In terms of preconsolidation pressure, p'_y, the yield surface can be rewritten as follows

$$\left(\frac{\eta}{M}\right)^n = -\frac{\ln\left(p'/p'_y\right)}{\ln r^*} \tag{8}$$

The variations of state boundary surfaces (equation (8)) with stress-state coefficient are shown in Fig. 2(b), with normalisation of preconsolidation pressure. Rowe's stress dilatancy relation (Rowe, 1962), as expressed by

$$\frac{\dot{\delta}^p}{\dot{\gamma}^p} = \frac{9\ (M - \eta)}{9 + 3M - 2M\eta} \times \frac{m}{m+1} \tag{9}$$

is adopted to define the plastic potential, which has been widely accepted as having the greatest success in describing the deformation of sands and other granular media. Note that the relationship between the volumetric and shear strains in this paper and the conventional definitions is given by $\dot{\delta}^p/\dot{\gamma}^p = \dot{\varepsilon}^p_p/\dot{\varepsilon}^p_q \times m/m+1$. The plastic potential can then be obtained by the integration of the stress dilatancy relation (equation (9)), and the plastic flow rule is shown to be non-associated. The hardening law is adopted based on a typical isotropic volumetric plastic strain hardening, as shown to be

$$p'_y = \frac{v p'_y}{\lambda - \kappa}\dot{\delta}^p \tag{10}$$

ANALYTICAL SOLUTION

The analytical solution is provided in this section, for a cavity expanded from a_0 to a until the soil around the cavity reaches the critical state (i.e. soil medium is deformed to have elastic, plastic and critical-state regions). 'c' is the radius of the elastic plastic boundary, and c_{cs} is the radius where the soil starts to be in critical state. Thus, for $r > c$, soil is in the elastic region; whereas for $c_{cs} < r < c$, the soil is in the plastic region, and the critical-state zone is for soil at $a < r < c_{cs}$ (see Fig. 1).

Solution for soil in elastic region

In terms of the undrained condition, the soil volume within an arbitrary radius (r) can be assumed as constant ($\dot{\varepsilon}_p = 0$), and the relation can be written as

$$r^{m+1} - r_0^{m+1} = a^{m+1} - a_0^{m+1} = T \tag{11}$$

where T is the variable representing the volumetric change at an arbitrary radius. To describe the stress strain relationship in the elastic region, the elastic strain rates are expressed as follows

$$\begin{aligned} \dot{\delta}^e &= \frac{1}{K}\dot{p}' \\ \dot{\gamma}^e &= \frac{1}{2\ G}\dot{q} \end{aligned} \tag{12}$$

where K is the elastic bulk modulus, which is equal to vp'/κ; G is the elastic shear modulus, which is determined by $(1+m)(1-2\mu)vp'/\{2[1+(m-1)\mu]\ \kappa\}$ (the derivation of isotropic linear elastic material can be found in Collins & Stimpson (1994)). In the elastic region, the elastic volumetric strain rate equals the total volumetric strain rate ($\dot{\delta} = \dot{\delta}^e = 0$); thus the mean stress rate is zero based on equation (12), and $p' = p'_0$.

For the cumulative changes since the initial condition, the radial and tangential stresses can be written as: $\sigma'_r = p'_0 + \Delta\sigma'_r$; $\sigma'_\theta = p'_0 + \Delta\sigma'_\theta$. Thus, $\Delta\sigma'_r = -m\ \Delta\sigma'_\theta$, based on the relation of $\dot{p}' = 0$. $\Delta\sigma'_\theta$ can then be derived as a function of radius r, based on equations (2), (3), (12)

$$\begin{aligned} \Delta\sigma'_\theta &= 2G_0\varepsilon_\theta = 2G_0\ \ln\left(\frac{r_0}{r}\right) \\ &= \frac{2G_0}{m+1}\ \ln\left(\frac{r^{m+1} - T}{r^{m+1}}\right) = A(r) \end{aligned} \tag{13}$$

With the aid of equilibrium equation (1), the incremental form of the radial total stress can be obtained as

$$\begin{aligned} \partial\sigma_r &= \frac{m\ (m+1)}{r}A(r)\partial r \\ &= 2G_0 m\frac{\ln[(r^{m+1} - T)/r^{m+1}]}{r}\partial r \end{aligned} \tag{14}$$

The integration of equation (14) from r to $r = \infty$ gives

$$\sigma_r - p_0 = 2G_0 m\int\frac{\ln[(r^{m+1} - T)/r^{m+1}]}{r}\partial r \tag{15}$$

and introducing the series expansion ($\ln x = -\sum_{k\ 1}^{\infty}(-1)^k \times(-1+x)^k/k$ for $0 < x < 2$) leads to the following expression

$$\int\frac{\ln\left[\left(r^{m+1} - T\right)/r^{m+1}\right]}{r}\partial r = \frac{1}{m+1}\sum_{k\ \ 1}^{\infty}\left(T/r^{m+1}\right)^k/k^2 = B(r) \tag{16}$$

Therefore, the distributions of stresses and strains in the elastic zone are formulated as follows

$$\begin{aligned} \sigma'_r &= p'_0 - mA(r) \\ \sigma'_\theta &= p'_0 + \ A(r) \\ \Delta u &= (2G_0)mB(r) + mA(r) \\ \varepsilon_r &= -\ m/(2G_0) \times A(r) \\ \varepsilon_\theta &= 1/(2G_0)\ \times A(r) \end{aligned} \tag{17}$$

For soil at the elastic plastic boundary ($r=c$), the stress state is on the initial yield surface (i.e. $p'=p'_0$; $q=q|_{r=c}$; $p'_y=p'_{y0}$). With the yield surface function (equation (8)), the deviatoric stress ($q|_{r=c}$) is derived as

$$q|_{r=c}=\left(\frac{\ln R_0}{\ln r^*}\right)^{1/n} M p'_0 \tag{18}$$

On the other hand, the deviatoric stress can be obtained from the distributions in the elastic region (equation (17))

$$q|_{r=c}=-(m+1)A(c)=-2G_0\ \ln\left(\frac{c^{m+1}-T}{c^{m+1}}\right) \tag{19}$$

Combining equations (18) and (19) gives

$$c=\left\{\frac{T}{1-\exp\left[-(\ln R_0/\ln r^*)^{1/n}\dfrac{M p'_0}{2G_0}\right]}\right\}^{1/(m+1)} \tag{20}$$

$$c_0=\left(c^{m+1}-T\right)^{1/(m+1)}$$

T_{yield} can be solved from equation (20) for $c=a$, which is used to indicate the plastic stage when $T>T_{\text{yield}}$.

Solution for soil in plastic region

When soil is in the plastic region ($c_{\text{cs}}<r<c$), the elastic moduli (K and G) are not constant but functions of mean effective stress p'; and the undrained condition gives: $\delta^{\text{p}}=-\delta^{\text{e}}$. Following the integrations from $r=c$ to r, the elastic and plastic volumetric strains (equation (21)) are derived based on the elastic modulus (equation (12)) and the hardening relation (equation (10)), respectively

$$\begin{aligned}\delta^{\text{e}}&=\int \mathrm{d}\delta^{\text{e}}=\int_{p'_0}^{p'}\frac{\kappa}{v}\frac{1}{p'}\mathrm{d}p'=\frac{\kappa}{v}\ \ln\left(\frac{p'}{p'_0}\right)\\ \delta^{\text{p}}&=\int \mathrm{d}\delta^{\text{p}}=\int_{p'_{y0}}^{p'_y}\frac{\lambda-\kappa}{v}\frac{1}{p'_y}\mathrm{d}p'_y=\frac{\lambda-\kappa}{v}\ \ln\ \left.\frac{p'_y}{p'_{y0}}\right)\end{aligned} \tag{21}$$

Combining equations (21) and (8) gives

$$\left(\frac{\eta}{M}\right)^n=A_1+A_2\times\ln p' \tag{22}$$

where

$$\begin{aligned}A_1&=\frac{\ln R_0+\Lambda^{-1}\ln p'_0}{\ln r^*}\\ A_2&=-\frac{\Lambda^{-1}}{\ln r^*}\\ \Lambda&=\frac{\lambda-\kappa}{\lambda}\end{aligned} \tag{23}$$

The differential forms of q and $\ln p'_y$ are obtained based on the differentiation of equation (22), and expressed as follows

$$\begin{aligned}\mathrm{d}q&=M\times\left\{[A_1+A_2\times\ln p']^{1/n}+\frac{A_2}{n}[A_1+A_2\times\ln p']^{1/n-1}\right\}\mathrm{d}p'\\ \mathrm{d}\ \ln p'_y&=\frac{\kappa}{\kappa-\lambda}\mathrm{d}\ \ln p'=\frac{\kappa}{\kappa-\lambda}\frac{n}{A_2M^n}\eta^{n-1}\mathrm{d}\eta\end{aligned} \tag{24}$$

Together with the boundary condition: $\gamma^{\text{e}}|_{r=c}=-(m+1)/(2G_0)A(c)$ based on equation (17), the elastic deviatoric strain (γ^{e}) is obtained through the integration

$$\begin{aligned}\int \mathrm{d}\gamma^{\text{e}}&=\gamma^{\text{e}}-\gamma^{\text{e}}|_{r=c}=\frac{[1+(m-1)\mu]\ \kappa}{(1+m)(1-2\mu)\ v}\int_{q|_{r=c}}^{q}\frac{1}{p'}\mathrm{d}q\\ &=\frac{[1+(m-1)\mu]\ \kappa M}{(1+m)(1-2\mu)\ v}\left\{\frac{n}{(1+n)A_2}[A_1+A_2\times\ln p']^{1/n+1}\right.\\ &\quad+[A_1+A_2\times\ln p']^{1/n}-\frac{n}{(1+n)A_2}\\ &\quad\left.\times[A_1+A_2\times\ln p'_0]^{1/n+1}-[A_1+A_2\times\ln p'_0]^{1/n}\right\}\end{aligned} \tag{25}$$

The integration of the plastic deviatoric strain (γ^{p}) is derived with the aid of the stress dilatancy relation (equation (9))

$$\begin{aligned}\gamma^{\text{p}}&=\int_{\ln p'_{y0}}^{\ln p'_y}\frac{(9+3M-2M\eta)(\lambda-\kappa)(m+1)}{9v(M-\eta)m}\mathrm{d}\ \ln p'_y\\ &=\frac{-\kappa n(m+1)}{9vA_2M^nm}\left\{\frac{2M}{n}\left[\eta^n-\eta_c^n\right]+\left(9+3M-2M^2\right)\right.\\ &\quad\left.\times\int_{\eta_c}^{\eta}\frac{\eta^{n-1}}{M-\eta}\mathrm{d}\eta\right\}\end{aligned} \tag{26}$$

where $\eta_c=q|_{r=c}/p'_0$, and

$$\int\frac{\eta^{n-1}}{M-\eta}\mathrm{d}\eta=\begin{cases}0 & (\eta_c=M)\\ \dfrac{\eta^n}{M}\displaystyle\sum_{k=0}^{\infty}\left[\frac{1}{n+k}\times\left(\frac{\eta}{M}\right)^k\right] & (\eta_c<M)\\ \displaystyle\sum_{k=0}^{\infty}\left[-M^k\frac{\eta^{n-1-k}}{n-1-k}\right] & (\eta_c>M)\end{cases} \tag{27}$$

When the plastic potential is defined by the associated flow rule of the standard Cam-clay model: $\dot{\delta}^{\text{p}}/\dot{\gamma}^{\text{p}}=(M-\eta)\times m/(m+1)$, the plastic deviatoric strain can be derived as

$$\gamma^{\text{p}}=\frac{-\kappa n(m+1)}{vA_2M^nm}\int_{\eta_c}^{\eta}\frac{\eta^{n-1}}{M-\eta}\mathrm{d}\eta \tag{28}$$

For a soil element at an arbitrary position (r) in the plastic region, the radial and tangential strains can be obtained based on the kinematic relationship of undrained expansion. Hence the distributions of radial and tangential stresses can be described by combining equations (3), (21), (25) and (26), according to the relation of $\gamma=\gamma^{\text{e}}+\gamma^{\text{p}}$. However, to obtain the total stresses and the excess pore water pressure, a numerical integration is required based on the equilibrium equation (1)

$$\int\partial\sigma_{\text{r}}=-m\int\frac{q}{r}\mathrm{d}r \tag{29}$$

Solution for soil in critical-state region

When the cavity is expanded further, critical state is reached for the soil close to the cavity. The boundary of the critical state soil is referred as to c_{cs}, and the critical-state region is for soil where $a<r<c_{\text{cs}}$. In the critical-state region,

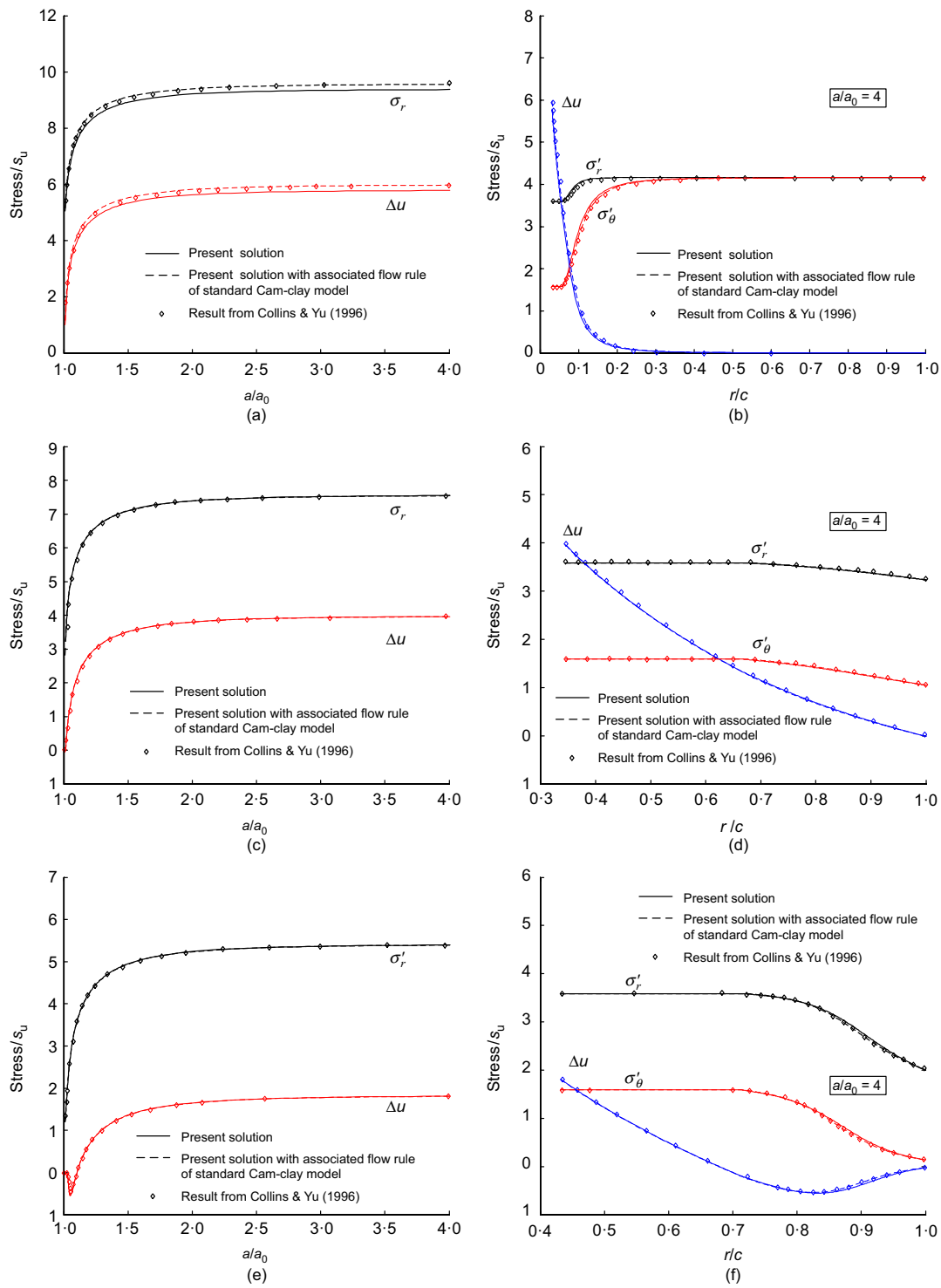

Fig. 3. Spherical cavity expansion curves and stress distributions, with variation of the overconsolidation ratio, R_0: (a) spherical cavity expansion curves for overconsolidation ratio (OCR) of $R_0 = 1$; (b) stress distributions in plastic/failure region for $R_0 = 1$; (c) spherical cavity expansion curves for OCR of $R_0 = 4$; (d) stress distributions in plastic/failure region for $R_0 = 4$; (e) spherical cavity expansion curves for OCR of $R_0 = 16$; (f) stress distributions in plastic/failure region for $R_0 = 16$

the deviatoric and mean effective stresses are constant, and expressed as

$$p'_{cs} = \left(\frac{R_0}{r^*}\right)^{\Lambda} p'_0 = \exp\left[\frac{\Gamma - v}{\lambda}\right]$$

$$q_{cs} = p'_{cs} \times M \tag{30}$$

$$p'_{y,cs} = p'_{cs} \times r^* = \left(\frac{R_0}{r^*}\right)^{\Lambda} r^* p'_0$$

Considering the scenario of infinite expansion (i.e. $a = \infty$), the limit solution of cavity pressure can be achieved by taking the plastic region as the critical state region, since $c_{cs} \approx c$ for infinite expansion. Thus the limit cavity pressure can be simplified from equation (29) and expressed as

$$\sigma_r|_{r\ a,\lim} = \sigma_r|_{r\ c} = -mq_{cs}\ \ln\frac{a}{c} \tag{31}$$

where c and $\sigma_r|_{r\ c}$ are given by equations (20) and (17), as functions of cavity radius a. Regardless of cavity radius, the

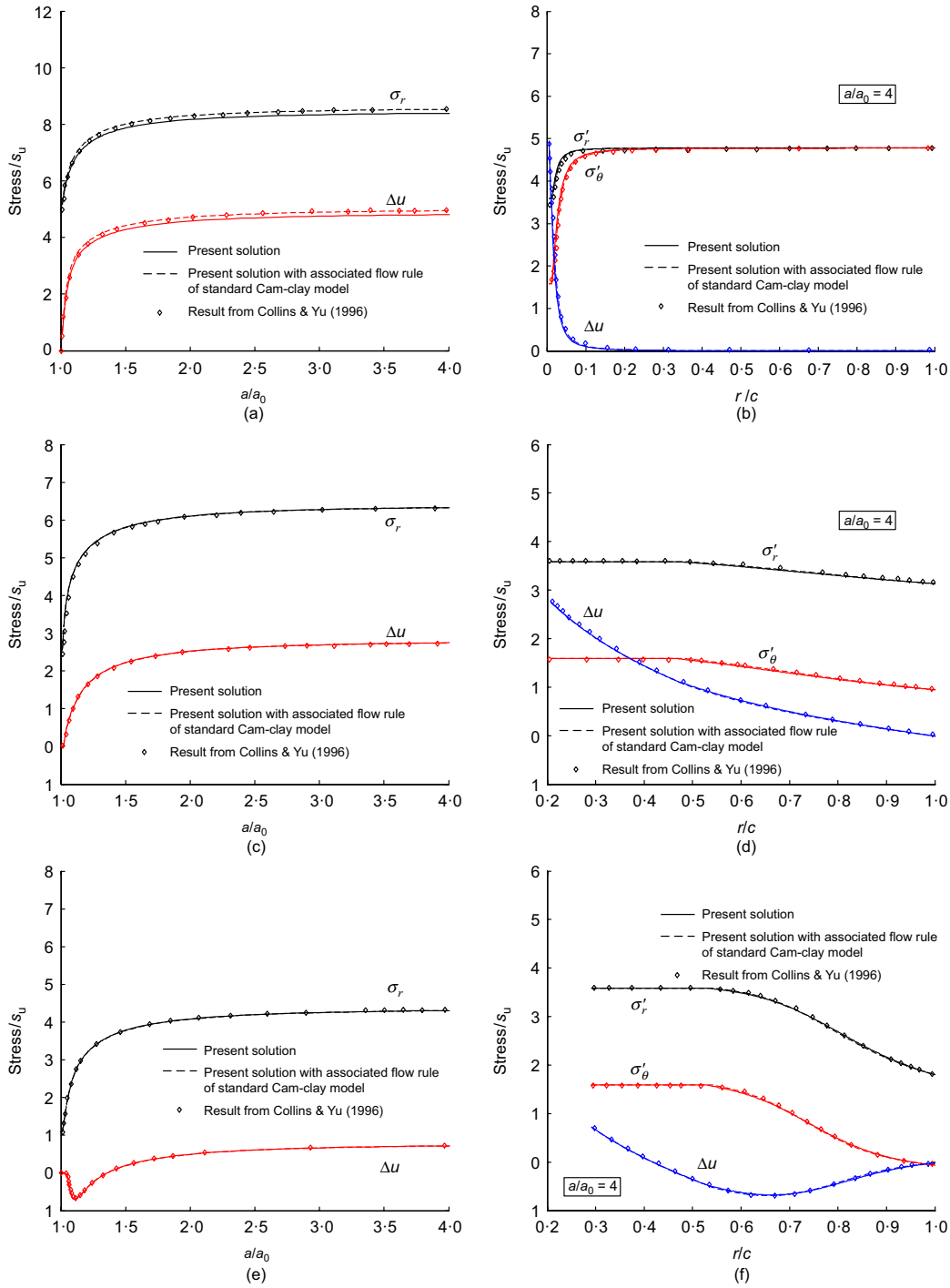

Fig. 4. Cylindrical cavity expansion curves and stress distributions, with variation of the overconsolidation ratio, R_0: (a) cylindrical cavity expansion curves for OCR of $R_0 = 1$; (b) stress distributions in plastic/failure region for $R_0 = 1$; (c) cylindrical cavity expansion curves for OCR of $R_0 = 4$; (d) stress distributions in plastic/failure region for $R_0 = 4$; (e) cylindrical cavity expansion curves for OCR of $R_0 = 16$; (f) stress distributions in plastic/failure region for $R_0 = 16$

limit cavity pressure can also be presented explicitly as

$$\sigma_r|_{r\ a,\lim} = p'_0 - \frac{m}{m+1} q_{cs} \ln A_3 + 2G_0 m A_4 \tag{32}$$

where

$$A_3 = \frac{T}{c^{m+1}} = 1 - \exp\left[-\left(\frac{\ln R_0}{\ln r^*}\right)^{1/n} \times \frac{Mp'_0}{2G_0}\right]$$
$$A_4 = B(c) = \frac{1}{m+1}\sum_{k=1}^{\infty}\frac{A_3^k}{k^2} \tag{33}$$

RESULTS AND DISCUSSION

In this section, results based on the analytical solution are presented for both spherical and cylindrical cavity expansion in soils under undrained condition. Unless stated otherwise, the material parameters are chosen to be relevant for London Clay: $\Gamma = 2{\cdot}759$, $\lambda = 0{\cdot}161$, $\kappa = 0{\cdot}062$, the critical state friction angle $\phi'_{cs} = 22{\cdot}75°$; according to Wood (1990) and Collins & Yu (1996). The Poisson ratio μ is assumed to be 0·3, and the specific volume of the soil v is equal to 2·0. The frictional constant M is determined by the critical state friction angle, using $M = 6\sin\phi'_{cs}/(3 - \sin\phi'_{cs})$ for spherical cavities and $M = 2\sin\phi'_{cs}$ for cylindrical cavities (Wood, 1990). The

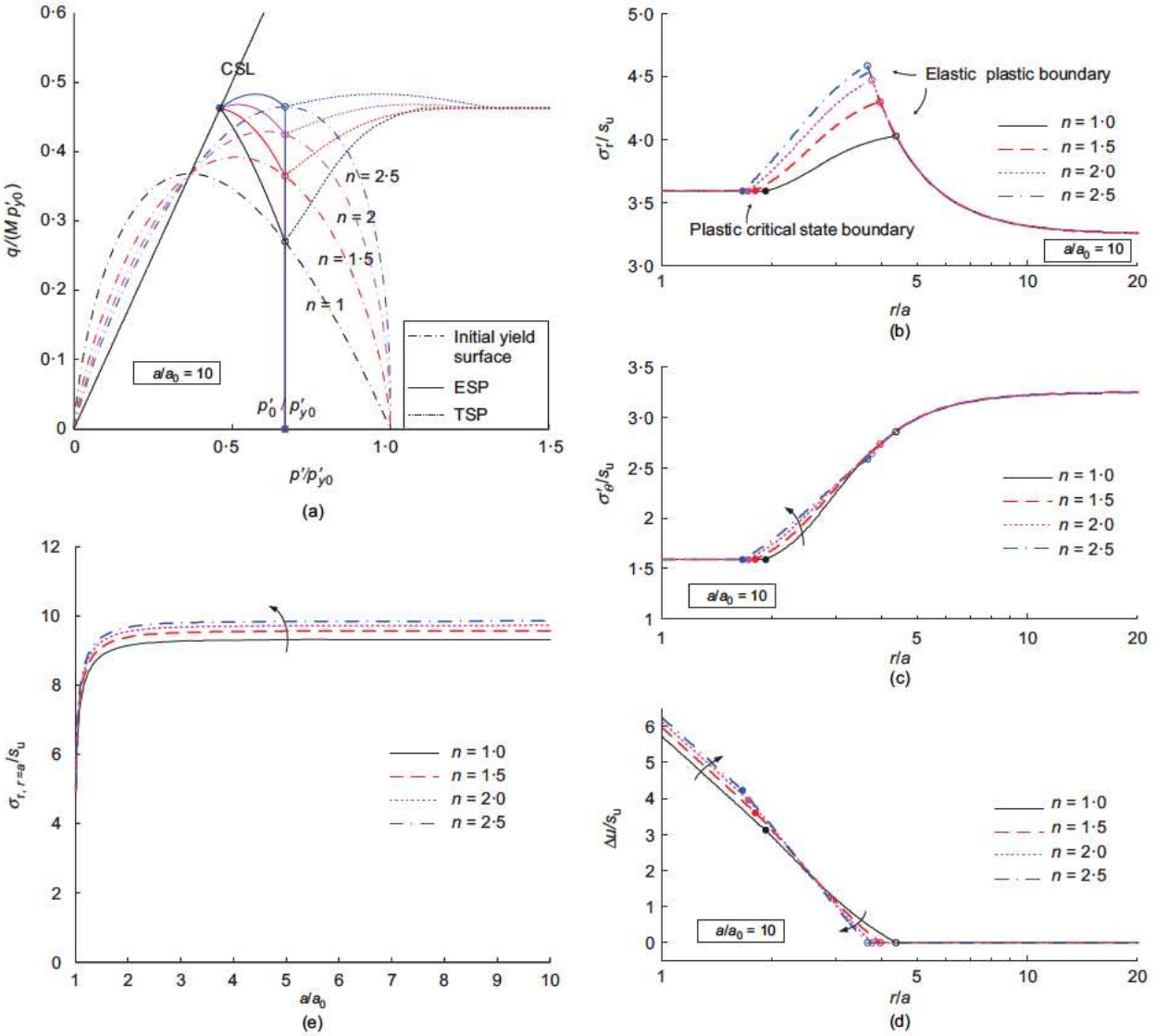

Fig. 5. Variations of cavity expansion results with the stress state coefficient n for $R_0 = 1{\cdot}5$: (a) stress paths at cavity wall; (b) radial stress distributions; (c) tangential stress distributions; (d) distributions of excess pore pressure; (e) spherical cavity expansion curves

undrained shear strength of the soil is defined as $s_u = 0{\cdot}5M \exp[(\Gamma - \upsilon)/\lambda]$, based on the Mohr circle of effective stresses at failure. For all the results of total stresses, ambient pore pressure is not included (i.e. $\sigma = \sigma' + \Delta u$).

Results of original Cam-clay model

It needs to be noted that the yield criterion of the original Cam-clay model can be recovered from CASM by selecting the material constants: $n = 1{\cdot}0$ and $r^* = 2{\cdot}7183$. Therefore the validation of this proposed solution is carried out by comparing the results of original Cam-clay model with the data from Collins & Yu (1996), as shown in Figs 3 and 4.

Figures 3(a), 3(c) and 3(e) present the spherical cavity expansion curves of a/a_0 from 1 to 4, for overconsolidation ratio of $R_0 = 1$, 4, 16. Both cavity pressure (σ_r) and excess pore pressure at the cavity wall (Δu) increase rapidly and seem to reach limit values, except for the case of heavily overconsolidated soil, which experiences negative excess pore pressure in the early stage of expansion with the generation of the plastic region. Both σ_r and Δu decrease with the overconsolidation ratio R_0, whereas the ultimate differences of these two stresses are identical, because the effective stresses at critical state are independent of R_0 (equation (30)).

Correspondingly, the stress distributions in the plastic/critical-state region ($a < r < c$) for overconsolidation ratio of $R_0 = 1$, 4, 16, are shown in Figs 3(b), 3(d) and 3(f), at the instant of $a/a_0 = 4$. Although the effective stresses (σ'_r, σ'_θ) at the cavity wall are the same with the variation of overconsolidation ratio, the stress distributions around the cavity differ with each other in the plastic and elastic regions. It is also clear to see that the excess pore pressure is developed continually in the critical-state region. Similarly, the results of cylindrical cavity expansion with the original Cam-clay model are presented in Fig. 4.

The comparisons with the data from Collins & Yu (1996) indicate that the results from two effective-stress analytical solutions for the original Cam-clay model are generally comparable. The small amount of difference in the results mainly comes from the stress dilatancy relation. In Collins & Yu (1996), the associated flow rule was applied to simplify the derivation; whereas Rowe's stress dilatancy relation (equation (9)) is used in the current solution, which represents a non-associated flow rule, and is able to describe the behaviour of sands and clays. However, it is also found that identical results are obtained by modifying the solution in the earlier section 'Analytical solution' by using the associated flow rule of the standard Cam-clay model (equation (28)).

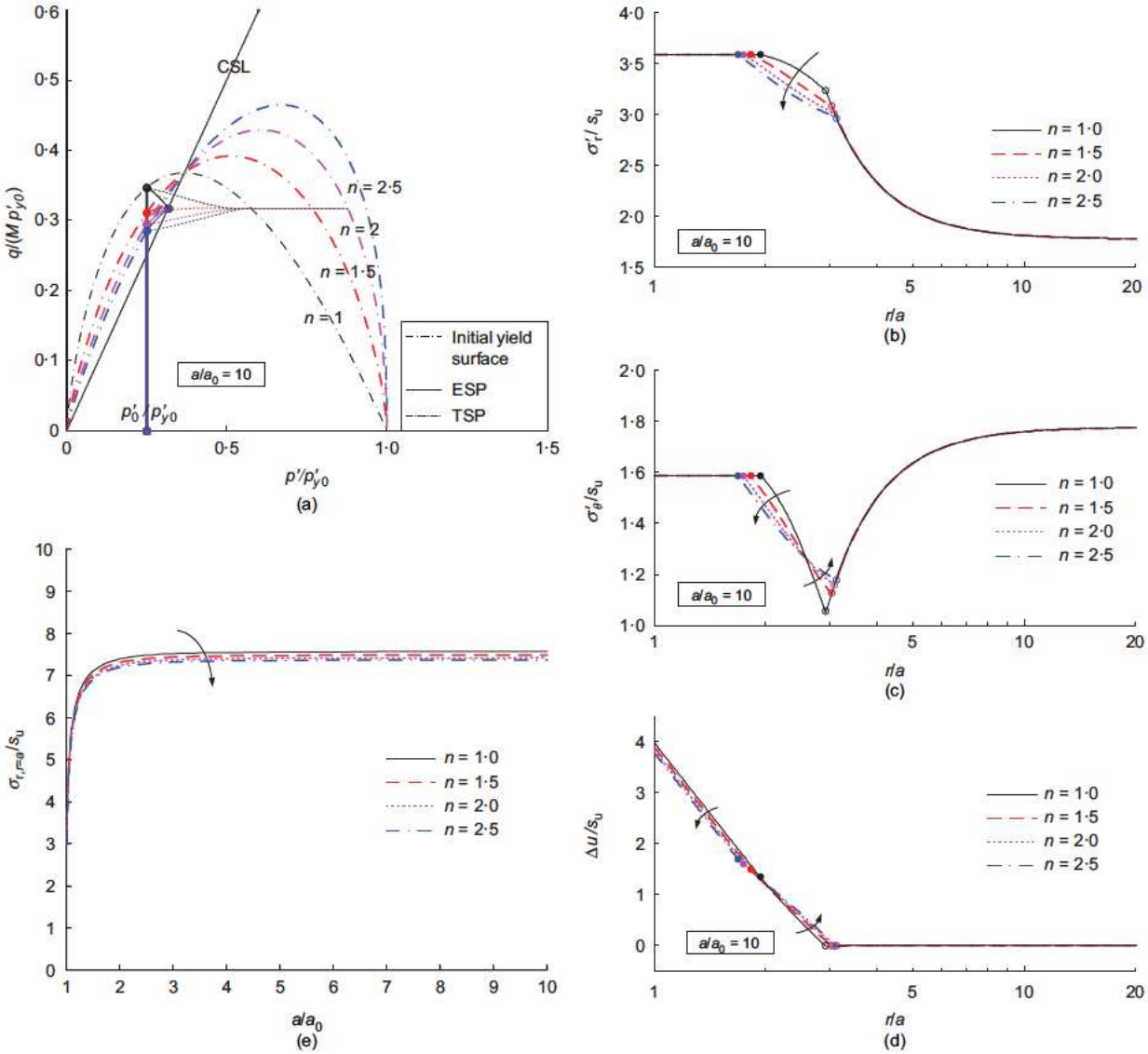

Fig. 6. Variations of cavity expansion results with the stress state coefficient n for $R_0 = 4$. (a) stress paths at cavity wall; (b) radial stress distributions; (c) tangential stress distributions; (d) distributions of excess pore pressure; (e) spherical cavity expansion curves

On the other hand, the good agreement of the results shows the validation of the newly proposed solution, and the solution with two additional material parameters of CASM provides more accurate analysis of soil behaviour in undrained cavity expansion.

Results with variations of stress-state coefficient and spacing ratio

A parametric study of cavity expansion using the unified soil model is provided in this section. Compared with the standard Cam-clay models, CASM introduced two new material constants: the stress-state coefficient (n) and the spacing ratio (r^*). The results of cavity expansion are presented with variation of n and r^*, for the cases of $R_0 = 1{\cdot}5$ and 4. The scenario of spherical cavity expansion is applied for the parametric study of stress paths, stress distributions and cavity expansion curves.

Figures 5(a) and 6(a) show the stress paths from $a/a_0 = 1$ to 10 at a cavity wall for the overconsolidation ratio of $R_0 = 1{\cdot}5$ and 4, respectively. The effective stresses are normalised by the preconsolidation pressure p'_{y0}, and the stress paths are plotted in $q/(M\,p'_{y0}) - p'_0/p'_{y0}$ space. With the variation of n from 1·0 to 2·5 (the spacing ratio is chosen as 2·7183), the shape of the initial yield surface varies, while the intersection with the critical state line (CSL) is independent of n when $\eta = M$. Initial mean effective stresses start from $p'_0/p'_{y0} = 0{\cdot}667$ and 0·25, and keep constant in the elastic stage due to the zero elastic volumetric strain (equation (12)). The effective stress paths (ESPs) and total stress paths (TSPs) overlap in the elastic stage, as the excess pore pressure Δu is very close to zero (equation (17)). Note that the excess pore pressure in the elastic region is small but not identical to zero, as the large strain assumption is used in this paper (see Collins & Yu, 1996). In contrast, the small strain assumption used by most previous researchers (e.g. Timoshenko & Goodier, 1970; Yu, 2000; Chen & Abousleiman, 2012) leads to zero excess pore pressure in the elastic region. In the plastic stage, the stress paths develop from the initial yield state to the critical state, which is also independent of n; large excess pore pressure is observed from the difference of TSP and ESP. Further development of Δu is shown in the critical-state stage, whereas the effective stresses remain constant at the critical state.

Effective stress distributions at $a/a_0 = 10$ are provided in Figs 5(b), 5(c) and 6(b), 6(c), for $R_0 = 1{\cdot}5$ and 4, respectively. The stresses ($\sigma'_r, \sigma'_\theta$) are normalised by the undrained shear strength s_u, and the radial position r is normalised by the

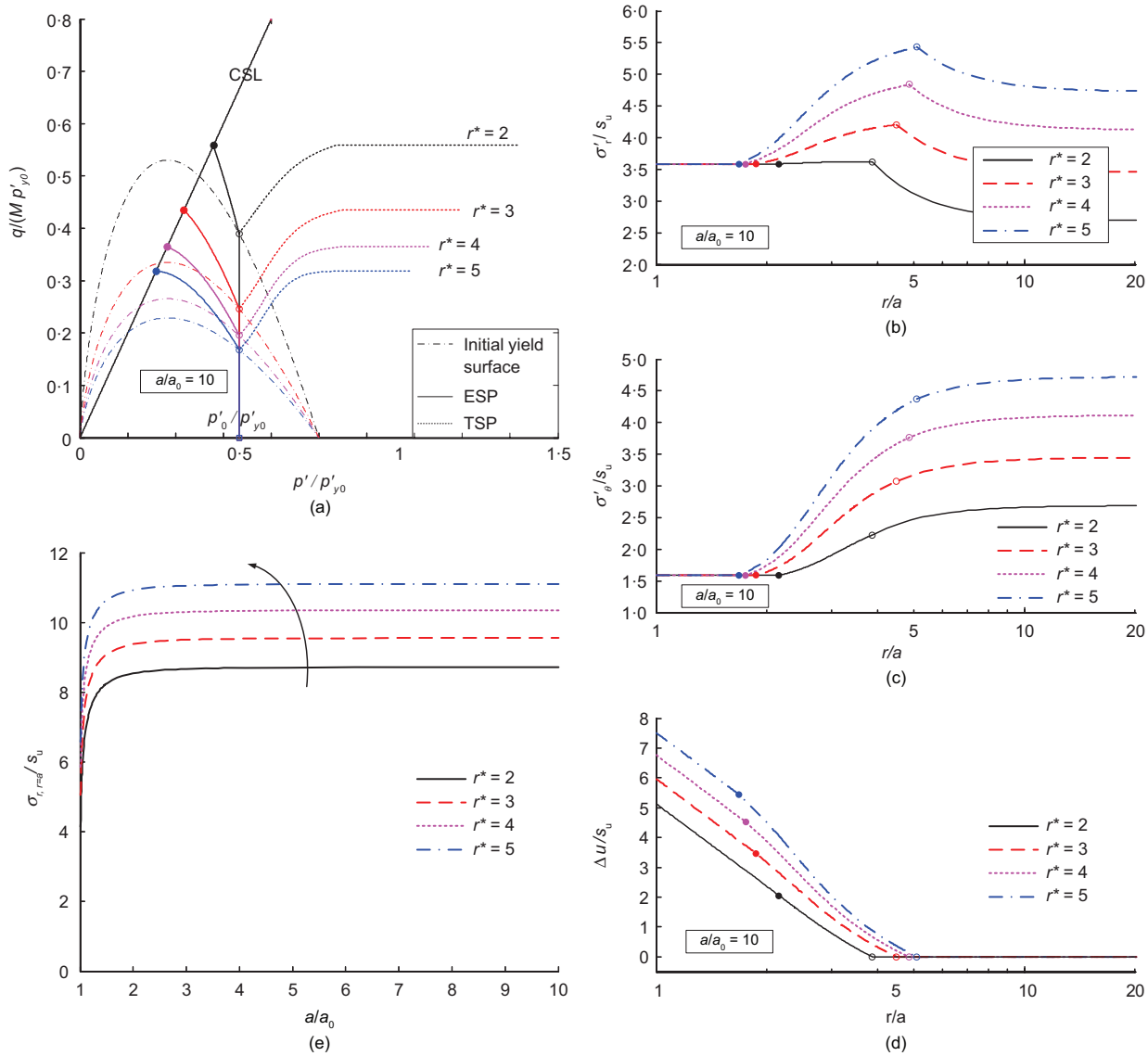

Fig. 7. Variations of cavity expansion results with the spacing ratio r^* for $R_0 = 1{\cdot}5$: (a) stress paths at cavity wall; (b) radial stress distributions; (c) tangential stress distributions; (d) distributions of excess pore pressure; (e) spherical cavity expansion curves

cavity radius a and plotted in logarithmic scale. The distributions of σ'_r and σ'_θ overlap in the elastic and critical-state regions, while the effective stresses vary in the plastic regions. It should be noted that both σ'_r/s_u and σ'_θ/s_u in the critical-state regions are independent of n and R_0. Since the undrained shear strength s_u is equivalent to $p'_{cs}/2$, the critical value of σ'_r/s_u can be derived as $2/M + 2m/(1+m)$, and $\sigma'_{\theta,cs}/s_u = 2/M - 2/(1+m)$. Therefore, the critical values are 3·586 and 1·586, respectively, for the spherical scenario. For $R_0 = 1{\cdot}5$, both σ'_r and σ'_θ increase with n in the plastic region, whereas σ'_r and σ'_θ generally decrease with n for $R_0 = 4$. The distributions of $\Delta u/s_u$ (Figs 5(d) and 6(d)) show the rapid growth of excess pore pressure in both the plastic and critical-state regions. For $R_0 = 1{\cdot}5$, Δu for soil close to the cavity wall increases with n, and the sizes of both plastic and critical-state regions (c and c_{cs}) decrease with n. For $R_0 = 4$, c_{cs} decreases with n, while c increases with n.

Figures 5(e) and 6(e) present the spherical cavity expansion curves for $a/a_0 = 1$ to 10. The radial stress at the cavity wall is normalised by the undrained shear strength s_u, and the radius of cavity a is normalised by the initial cavity radius a_0. The cavity pressure increases rapidly with expansion to a limit value, which increases with n for $R_0 = 1{\cdot}5$ and decreases with n for $R_0 = 4$.

Similarly, the results of spherical cavity expansion with variation of spacing ratio r^* are shown in Figs 7 and 8. Both $R_0 = 1{\cdot}5$ and 4 are presented to compare the effect of over-consolidation ratio; the spacing ratio varies from 2 to 5, and the stress-state coefficient remains as 1. As shown in Figs 7(a) and 8(a), the stress paths end at critical states, which are dependent on r^* (see equation (30)). A larger size of the yield surface is observed for smaller r^*, and both critical-state mean and deviatoric stresses are higher. For the cases of $R_0 = 4$ and $r^* = 4$, critical state is reached when the soil comes to the initial yield surface (i.e. the soil does not experience the plastic stage during undrained expansion). It is also clear to see the negative excess pore pressure in the early plastic stage for the case of $R_0 = 4$ and $r^* = 2$.

Figures 7(b), 7(c) and 8(b), 8(c) present the effective stress distributions with variation of r^*. The critical values of σ'_r/s_u and σ'_θ/s_u are also independent on r^*, and equal to 3·586 and 1·586, respectively. It needs to be noted that the undrained shear strength varies with the spacing ratio, according to the variation of critical state on CSL in Figs 7(a) and 8(a). Therefore, critical values of σ'_r and σ'_θ decrease with r^*.

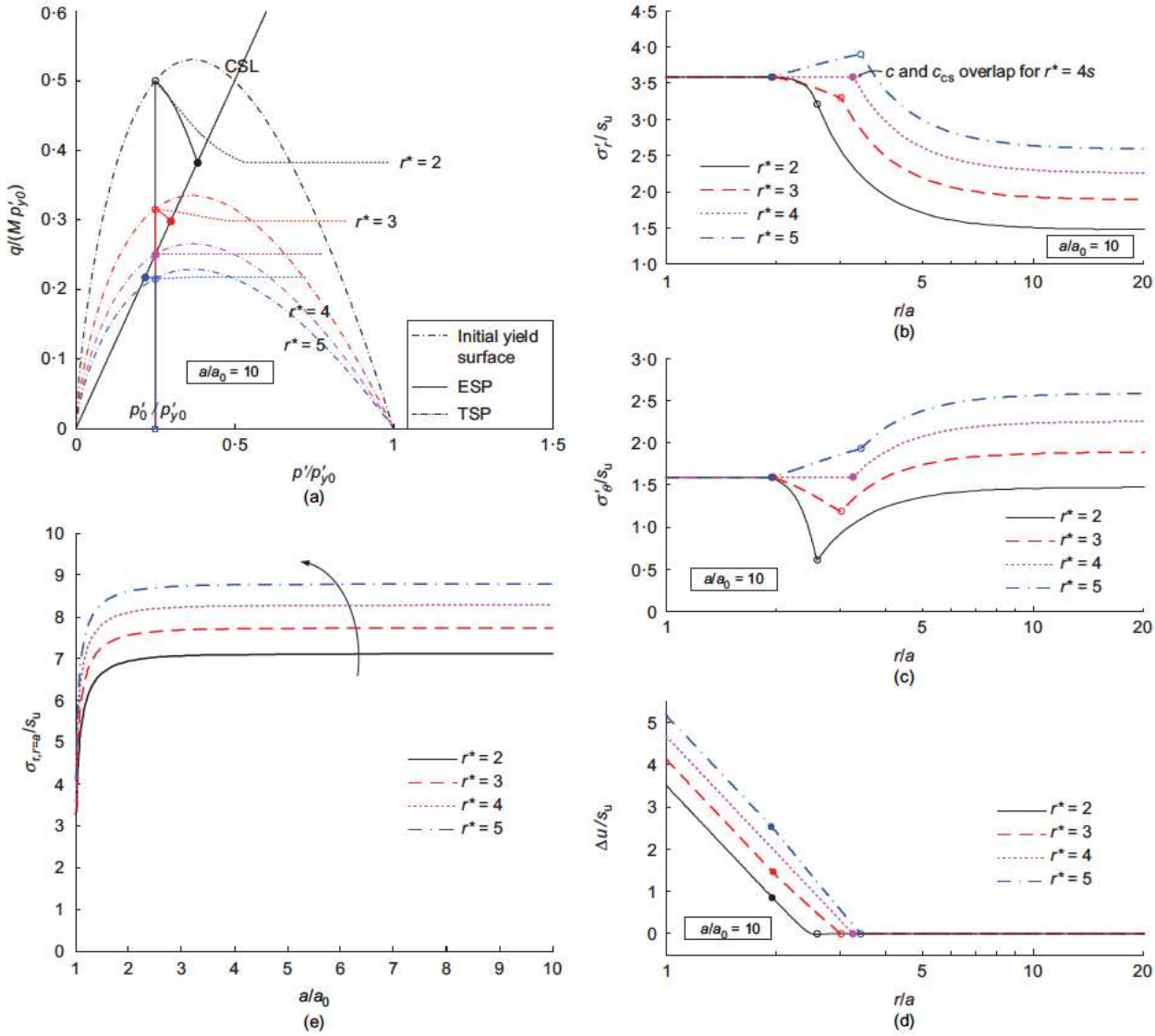

Fig. 8. Variations of cavity expansion results with the spacing ratio r^* for $R_0 = 4$: (a) stress paths at cavity wall; (b) radial stress distributions; (c) tangential stress distributions; (d) distributions of excess pore pressure; (e) spherical cavity expansion curves

For both $R_0 = 1{\cdot}5$ and 4, the size of the plastic region c increases with r^*. For the case of $R_0 = 4$ and $r^* = 4$, lines of c and c_{cs} overlap, showing no plastic region in the expanded soil. The cavity expansion curves in Figs 7(e) and 8(e) indicate that the excess pore pressure at the cavity wall increases with r^*, for scenarios of both $R_0 = 1{\cdot}5$ and 4.

Results of excess pore pressure at cylindrical cavity wall

To investigate the excess pore pressure generated at the pile soil interface during pile installation in clay soils, cylindrical cavity expansion showed its potential and usefulness in prediction of Δu for pile tests in both normally consolidated and heavily overconsolidated clays (e.g. Randolph *et al.*, 1979; Collins & Yu, 1996). The results of the variation of the normalised excess pore pressure at the cavity wall with the overconsolidation ratio are presented in this section using the proposed solution in the CASM model.

Figure 9(a) shows the result of cylindrical cavity expansion in original Cam-clay, which is compared with the data from Collins & Yu (1996). This curve also serves as a reference for later parametric study. The value of Δu is obtained at $a/a_0 = 4$, and normalised by the corresponding value of s_u. The degradation of $\Delta u/s_u$ with R_0 from 1 to 50 is observed, and has a good agreement with the data based on the solution of Collins & Yu (1996). Negative excess pore pressure is also shown when R_0 is larger than 31. The effect of initial specific volume is shown in Fig. 9(b), and higher specific volume results in a slightly higher normalised excess pore pressure. A similar trend was also reported by Collins & Yu (1996) using the modified Cam-clay model.

The influences of r^* and n are investigated and presented in Figs 9(c) and 9(d). It is found that the normalised excess pore pressure increases with the value of spacing ratio. Compared to the effects of r^*, the influence of stress-state coefficient n is relatively smaller. For normally consolidated and lightly overconsolidated soils, $\Delta u/s_u$ increases slightly with n. However, for heavily overconsolidated soils, the normalised excess pore pressure decreases with the stress-state coefficient. The reversal of the trend appears when R_0 is about 3. This trend also explains the variation of total radial stress at the cavity wall for $R_0 = 1{\cdot}5$ and 4 in Figs 5(d) and 6(d).

Application to self-boring pressuremeter

In this section, the analytical solution using CASM is applied to simulate the self-boring pressuremeter tests, which have been widely used to obtain fundamental soil properties,

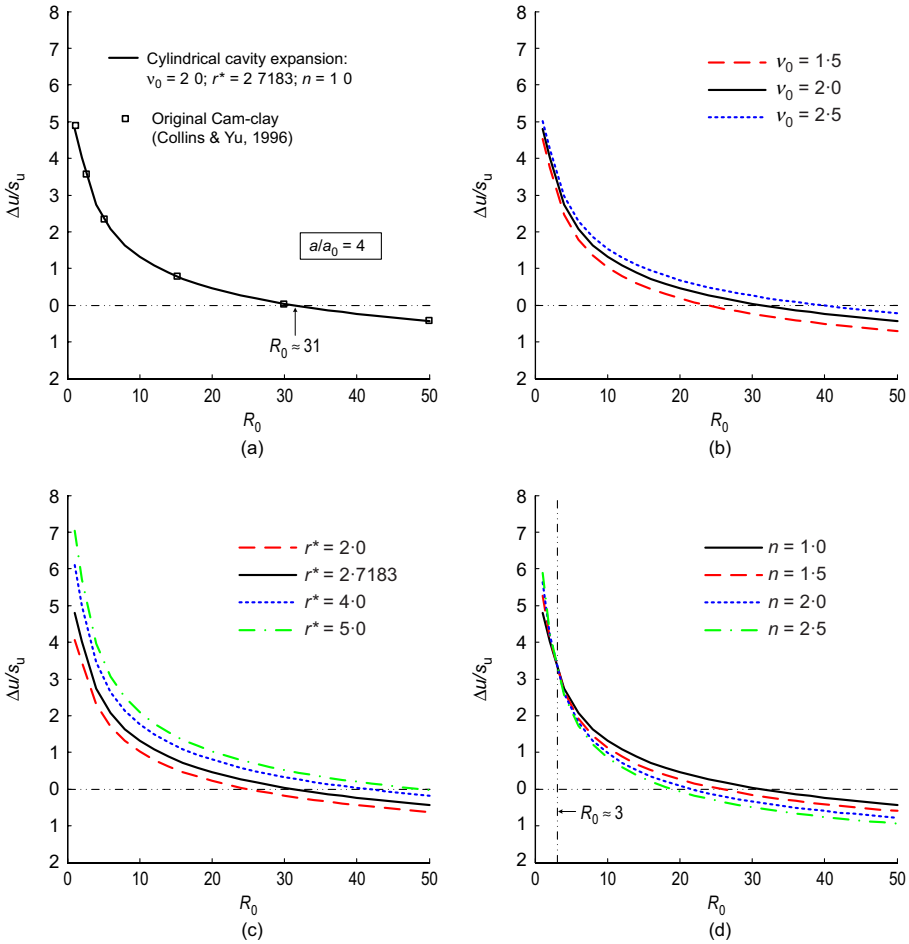

Fig. 9. Variations of excess pore pressure at cavity wall with the OCR, R_0: (a) comparison with Collins & Yu (1996); (b) effect of initial specific volume; (c) effect of spacing ratio; (d) effect of stress state coefficient

as one of the best in situ tests for geotechnical investigation (Wroth, 1984; Clarke, 1995; Yu, 2000). The pressure/displacement response from the inflated cylindrical membrane of the pressuremeter is analysed to determine soil parameters (e.g. undrained shear strength, shear modulus, consolidation coefficient, state parameter). Gibson & Anderson (1961) were among the first to propose a simple relationship between pressuremeter pressure (ψ) and undrained shear strength (s_u) using cavity expansion in a Tresca model, in which the plastic part of the pressuremeter loading curve has a linear relation within the log scale of volumetric strain

$$\psi = \psi_{\text{lim}} + s_u \times \ln\left(\frac{\Delta V}{V}\right) \tag{34}$$

where ψ_{lim} is the pressuremeter limit pressure and $\Delta V/V = (a^2 - a_0^2)/a^2$ is the volumetric strain. Note that this expression can also be recovered from this solution for infinite expansion (equations (31) and (32)).

Although the overestimation of s_u for normally consolidated clays using the interpretation procedure of Gibson & Anderson (1961) was reported by Clarke (1993), the analytical solution (Yu & Collins, 1998) and numerical simulation (Khong, 2004) suggested that the undrained shear strength using Gibson and Anderson's method was underestimated for heavily overconsolidated clays. Therefore, the proposed effective stress analysis is applied to investigate the interpretation of pressuremeter tests in both soft and stiff clays.

As Yu & Collins (1998) reported that initial specific volume (v) has little effect on the undrained shear strength derived from a pressuremeter test, the analysis in this section is focused on the effects of the soil parameters and the overconsolidation ratio. Regardless of the effect of pressuremeter geometry, the pressuremeter pressure ψ can be predicted as the radial stress at cavity wall $\sigma_r|_{r=a}$ for cylindrical expansion. Fig. 10(a) shows the normalised cavity pressure against the log-scale volumetric strain, in which the influence of stress-state coefficient n and overconsolidation ratio R_0 are investigated with a constant spacing ratio $r^* = 2{\cdot}7183$. The results indicate that the normalised pressuremeter pressure ψ/s_u increases slightly with stress-state coefficient n, while larger overconsolidation ratio decreases the value of ψ/s_u. However, the inclinations of the pressuremeter curves are comparable in the plastic stage. As suggested by Gibson & Anderson (1961), the derived undrained shear strength s_m from pressuremeter curves was obtained based on the stage for cavity strain $(a - a_0)/a_0$ between 5% and 15%.

The variation of the ratio of s_m to the theoretical triaxial undrained shear strength s_u with the value of overconsolidation ratio R_0 is presented in Fig. 10(b) for the effects of stress-state coefficient. It can be seen that the pressuremeter shear strength is close to the triaxial undrained shear strength for soft clays ($R_0 < 3$), and the ratio of shear strength s_m/s_u varies with R_0. For $n > 2{\cdot}0$, the derived shear strength s_m is smaller than the triaxial undrained shear strength s_u for heavily overconsolidated clays, which is also shown by a previous analytical solution (Yu & Collins, 1998) and numerical simulation (Khong, 2004). However, the results in Fig. 10(b) suggest that the value of n has a large influence on the variation of s_m/s_u with overconsolidation ratio R_0. Slightly overestimated shear strength for heavily overconsolidated clays is also found for $n = 1{\cdot}0$.

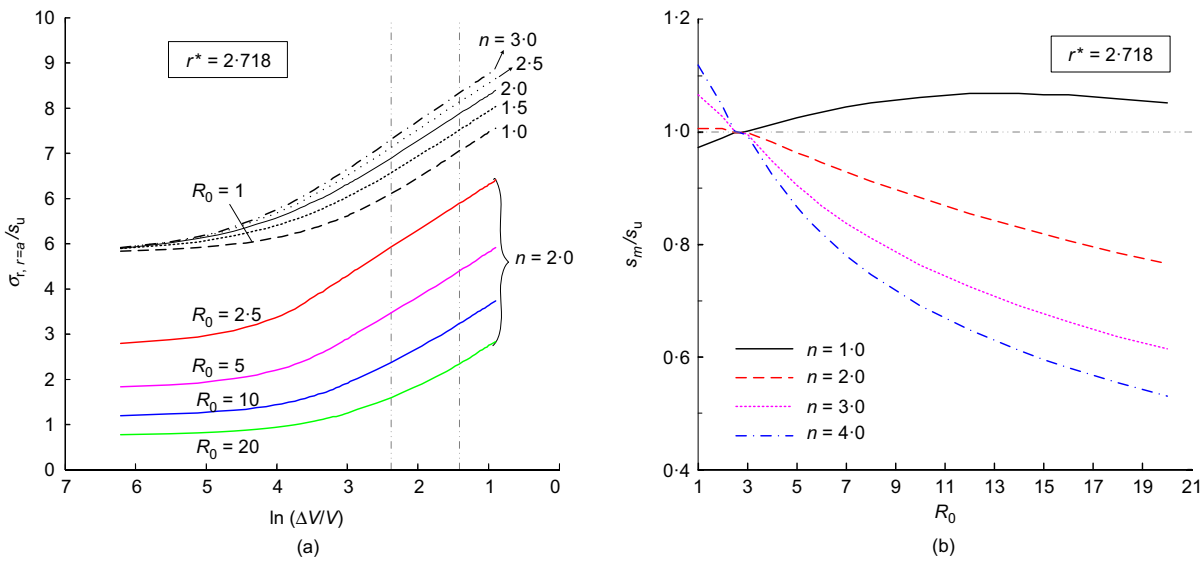

Fig. 10. Effects of stress state coefficient for $r^* = 2{\cdot}7183$: (a) pressuremeter loading curves; (b) variations of ratio of pressuremeter strength to triaxial undrained shear strength with R_0

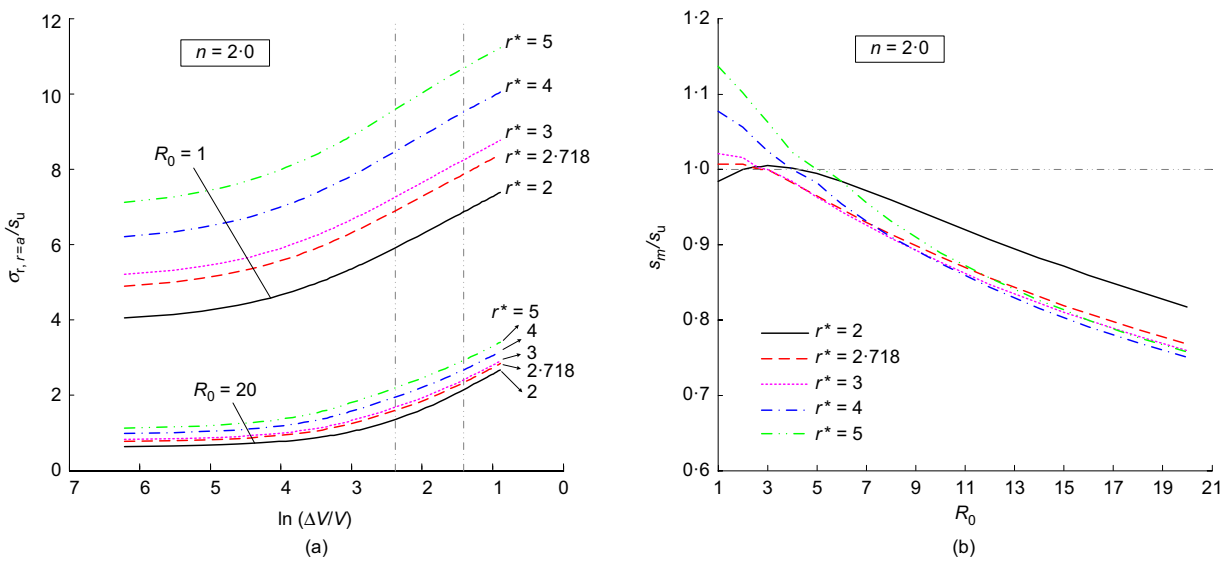

Fig. 11. Effects of spacing ratio for $n = 2{\cdot}0$: (a) pressuremeter loading curves; (b) variations of ratio of pressuremeter strength to triaxial undrained shear strength with R_0

Similarly, the influence of spacing ratio r^* on the results of a self-boring pressuremeter test is provided in Fig. 11. The spacing ratio has large effects on the increasing of the normalised pressuremeter pressure, especially for clays with smaller values of R_0 (Fig. 11(a)); while the influence of r^* is relatively small compared to that of the stress-state coefficient (Fig. 11(b)), with a similar decreasing trend of s_m/s_u against R_0. Therefore the more precise prediction of shear strength for clays is suggested by using the proposed cavity expansion solution and the evaluation of soil properties for CASM.

CONCLUSIONS

Undrained expansion of both spherical and cylindrical cavities with a unified state parameter model for clay and sand (CASM) is presented in this paper. CASM is a critical state soil model with two additional material constants (when compared with standard Cam clay models), which has the ability to capture the overall behaviour of clay and sand under both drained and undrained loading conditions. The complete analytical solution for large strain cavity expansion is derived for soil in the elastic, plastic and critical-state regions. The scenario of original Cam clay, as a special case of CASM, is recovered to compare with the data of previous study and validate the proposed solution, with the cavity expansion curves and stress distributions in the plastic region. The variations of stress-state coefficient and spacing ratio are investigated for the parametric study of stress paths, stress distributions and cavity expansion curves. Applications to pile installation and self-boring pressuremeter are provided, showing some practical insights into the prediction of excess pore pressure generated at the pile soil interface and the estimation of undrained shear strength based on the pressuremeter curves.

ACKNOWLEDGEMENTS

The authors would like to acknowledge financial support from the National Natural Science Foundation of China (no. 51323004) and 111 Project (B14021).

NOTATION

a	radius of cavity
c	radius of elastic/plastic boundary
c_{cs}	radius of critical state region boundary
e	void ratio of granular material
G	elastic shear modulus
K	elastic bulk modulus
M, κ, λ, Γ, Λ	critical state parameters
m	parameter to combine cylindrical (m 1) and spherical (m 2) analysis
n	stress state coefficient for CASM
p'	mean effective stress
p'_0	initial mean effective stress
p'_{y0}	preconsolidation pressure
q	deviatoric effective stress
R_0	isotropic overconsolidation ratio, defined as p'_{y0}/p'_0
r	radial position of soil element around cavity
r^*	spacing ratio for the concept of state parameter
s_m	derived undrained shear strength from pressure meter curve
s_u	undrained shear strength of soil
T	parameter for volumetric change of cavity, defined as a^{m+1} a_0^{m+1}
Δu	excess pore pressure
$\Delta V/V$	volumetric strain
δ, γ	volumetric and shear strains
ε_r, ε_θ	radial and tangential strains
η	stress ratio, defined as q/p'
μ	Poisson ratio of soil
v	specific volume, defined as $1+e$
ξ	state parameter
ξ_R	reference state parameter
σ'_θ, σ_θ	effective and total tangential stresses
σ'_r, σ_r	effective and total radial stresses
ϕ_{cs}	critical state friction angle
ψ	pressuremeter pressure

REFERENCES

Been, K. & Jefferies, M. G. (1985). A state parameter for sands. *Géotechnique* **35**, No. 2, 99 112, http://dx.doi.org/10.1680/geot.1985.35.2.99.

Cao, L. F., Teh, C. I. & Chang, M. F. (2001). Undrained cavity expansion in modified Cam clay I: theoretical analysis. *Géotechnique* **51**, No. 4, 323 334, http://dx.doi.org/10.1680/geot.2001.51.4.323.

Carter, J. P. (1978). *CAMFE: A computer program for the analysis of a cylindrical cavity expansion in soil*, Technical report. Cambridge, UK: Department of Engineering, University of Cambridge.

Carter, J. P., Booker, J. R. & Yeung, S. K. (1986). Cavity expansion in cohesive frictional soils. *Géotechnique* **36**, No. 3, 349 358, http://dx.doi.org/10.1680/geot.1986.36.3.349.

Chen, S. L. & Abousleiman, Y. N. (2012). Exact undrained elasto plastic solution for cylindrical cavity expansion in modified Cam Clay soil. *Géotechnique* **62**, No. 5, 447 456, http://dx.doi.org/10.1680/geot.11.P.027.

Chen, S. L. & Abousleiman, Y. N. (2013). Exact drained solution for cylindrical cavity expansion in modified Cam Clay soil. *Géotechnique* **63**, No. 6, 510 517, http://dx.doi.org/10.1680/geot.11.P.088.

Clarke, B. G. (1993). The interpretation of self boring pressuremeter tests to produce design parameters. In *Predictive soil mechanics* (eds G. T. Houlsby and A. N. Schofield), pp. 156 172. London, UK: Thomas Telford.

Clarke, B. G. (1995). *Pressuremeter in geotechnical design*. London, UK: Chapman and Hall.

Collins, I. F. & Stimpson, J. R. (1994). Similarity solutions for drained and undrained cavity expansions in soils. *Géotechnique* **44**, No. 1, 21 34, http://dx.doi.org/10.1680/geot.1994.44.1.21.

Collins, I. F. & Yu, H. S. (1996). Undrained cavity expansions in critical state soils. *Int. J. Numer. Analyt. Methods Geomech.* **20**, No. 7, 489 516.

Collins, I. F., Pender, M. J. & Wang, Y. (1992). Cavity expansion in sands under drained loading conditions. *Int. J. Numer. Analyt. Methods Geomech.* **16**, No. 1, 3 23.

Gibson, R. & Anderson, W. (1961). In situ measurement of soil properties with the pressuremeter. *Civ. Engng Public Works Rev.* **56**, No. 658, 615 618.

Khong, C. D. (2004). *Development and numerical evaluation of unified critical state models.* PhD thesis, University of Nottingham, Nottingham, UK.

Mo, P. Q., Marshall, A. M. & Yu, H. S. (2014). Elastic plastic solutions for expanding cavities embedded in two different cohesive frictional materials. *Int. J. Numer. Analyt. Methods Geomech.* **38**, No. 9, 961 977.

Palmer, A. C. & Mitchell, R. J. (1971). Plane strain expansion of a cylindrical cavity in clay. *Proceedings of the Roscoe memorial symposium*, Cambridge, UK, pp. 588 599.

Parry, R. H. G. (1956). *Strength and deformation of clay.* PhD thesis, University of London, London, UK.

Randolph, M. F., Carter, J. P. & Wroth, C. P. (1979). Driven piles in clay the effects of installation and subsequent consolidation. *Géotechnique* **29**, No. **4**, 361 393, http://dx.doi.org/10.1680/geot.1979.29.4.361.

Roscoe, K. H. & Schofield, A. N. (1963). Mechanical behaviour of an idealized wet clay. *Proceedings of the European conference on soil mechanics and foundation engineering*, Wiesbaden, Germany, vol. 1, pp. 47 54.

Roscoe, K. H., Schofield, A. N. & Wroth, C. P. (1958). On the yielding of soils. *Géotechnique* **8**, No. 1, 22 52, http://dx.doi.org/10.1680/geot.1958.8.1.22.

Rowe, P. W. (1962). The stress dilatancy relation for static equilibrium of an assembly of particles in contact. *Proc. R. Soc.* **269**, No. 1339, 500 527.

Schofield, A. N. & Wroth, C. P. (1968). *Critical state soil mechanics.* New York, NY, USA: McGraw Hill.

Sheng, D., Sloan, S. W. & Yu, H. S. (2000). Aspects of finite element implementation of critical state models. *Comput. Mech.* **26**, No. 2, 185 196.

Sladen, J. A. & Oswell, J. M. (1989). The behavior of very loose sand in the triaxial compression test. *Can. Geotech. J.* **26**, No. 1, 103 113.

Sladen, J. A., D'Hollander, R. D. & Krahn, J. (1985). The liquefaction of sands, a collapse surface approach. *Can. Geotech. J.* **22**, No. 4, 564 578.

Timoshenko, S. P. & Goodier, J. N. (1970). *Theory of elasticity.* New York, NY, USA: McGraw Hill.

Vesic, A. S. (1972). Expansion of cavities in infinite soil mass. *ASCE J. Soil Mech. Found. Div.* **98**(SM3), 265 290.

Wood, D. M. (1990). *Soil behaviour and critical state soil mechanics.* Cambridge, UK: Cambridge University Press.

Wroth, C. P. (1973). A brief review of the application of plasticity to soil mechanics. In *Plasticity and soil mechanics* (ed. A. C. Palmer), pp. 1 11. Cambridge, UK: Cambridge University Press.

Wroth, C. P. (1984). Interpretation of in situ soil tests. *Géotechnique* **34**, No. 4, 449 489, http://dx.doi.org/10.1680/geot.1984.34.4.449.

Yu, H. S. (1990). *Cavity expansion theory and its application to the analysis of pressuremeters.* PhD thesis, University of Oxford, Oxford, UK.

Yu, H. S. (1998). CASM: A unified state parameter model for clay and sand. *Int. J. Numer. Analyt. Methods Geomech.* **22**, No. 8, 621 653.

Yu, H. S. (2000). *Cavity expansion methods in geomechanics.* Dordrecht, the Netherlands: Kluwer Academic Publishers.

Yu, H. S. (2006). *Plasticity and geotechnics.* New York, NY, USA: Springer.

Yu, H. S. & Collins, I. F. (1998). Analysis of self boring pressuremeter tests in overconsolidated clays. *Géotechnique* **48**, No. 5, 689 693, http://dx.doi.org/10.1680/geot.1998.48.5.689.

Yu, H. S. & Houlsby, G. T. (1991). Finite cavity expansion in dilatant soils: loading analysis. *Géotechnique* **41**, No. 2, 173 183, http://dx.doi.org/10.1680/geot.1991.41.2.173.

Yu, H. S., Charles, M. T. & Khong, C. D. (2005). Analysis of pressuremeter geometry effects in clay using critical state models. *Int. J. Numer. Analyt. Methods Geomech.* **29**, No. 8, 845 859.